Publication Year	2020
Acceptance in OA@INAF	2021-01-19T12:32:02Z
Title	A Very Young Radio-loud Magnetar
Authors	Esposito, P.; Rea, N.; Borghese, A.; Zelati, F. Coti; Viganò, D.; et al.
DOI	10.3847/2041-8213/ab9742
Handle	http://hdl.handle.net/20.500.12386/29845
Journal	THE ASTROPHYSICAL JOURNAL LETTERS
Number	896

The Astrophysical Journal Letters, 896:L30 (8pp), 2020 June 20 https://doi.org/10.3847/2041-8213/ab9742
© 2020. The American Astronomical Society. All rights reserved.

A Very Young Radio-loud Magnetar

P. Esposito[1,2], N. Rea[3,4], A. Borghese[3,4], F. Coti Zelati[3,4], D. Viganò[3,4], G. L. Israel[5], A. Tiengo[1,2,6], A. Ridolfi[7,8], A. Possenti[7,9], M. Burgay[7], D. Götz[10], F. Pintore[2], L. Stella[5], C. Dehman[3,4], M. Ronchi[3,4], S. Campana[11], A. Garcia-Garcia[3,4], V. Graber[3,4], S. Mereghetti[2], R. Perna[12,13], G. A. Rodríguez Castillo[5], R. Turolla[14,15], and S. Zane[15]

[1] Scuola Universitaria Superiore IUSS Pavia, Palazzo del Broletto, piazza della Vittoria 15, I-27100 Pavia, Italy; paolo.esposito@iusspavia.it
[2] INAF—Istituto di Astrofisica Spaziale e Fisica Cosmica di Milano, via A. Corti 12, I-20133 Milano, Italy
[3] Institute of Space Sciences (ICE, CSIC), Campus UAB, Carrer de Can Magrans s/n, E-08193, Barcelona, Spain
[4] Institut d'Estudis Espacials de Catalunya (IEEC), Carrer Gran Capità 2-4, E-08034 Barcelona, Spain
[5] INAF—Osservatorio Astronomico di Roma, via Frascati 33, I-00078 Monteporzio Catone, Italy
[6] Istituto Nazionale di Fisica Nucleare (INFN), Sezione di Pavia, via A. Bassi 6, I-27100 Pavia, Italy
[7] INAF—Osservatorio Astronomico di Cagliari, Via della Scienza 5, I-09047 Selargius, Italy
[8] Max-Planck-Institute für Radioastronomie, Auf dem Hugel 69, D-53121 Bonn, Germany
[9] Department of Physics, Università di Cagliari, S.P. Monserrato-Sestu km 0,700, I-09042 Monserrato, Italy
[10] AIM-CEA/DRF/Irfu/Service d'Astrophysique, Orme des Merisiers, F-91191 Gif-sur-Yvette, France
[11] INAF—Osservatorio Astronomico di Brera, via E. Bianchi 46, I-23807 Merate (LC), Italy
[12] Department of Physics and Astronomy, Stony Brook University, Stony Brook, NY 11794, USA
[13] Center for Computational Astrophysics, Flatiron Institute, 162 5th Avenue, New York, NY 10010, USA
[14] Dipartimento di Fisica e Astronomia "Galileo Galilei", Università di Padova, via F. Marzolo 8, I-35131 Padova, Italy
[15] Mullard Space Science Laboratory, University College London, Holmbury St. Mary, Dorking, Surrey RH5 6NT, UK
Received 2020 April 8; revised 2020 May 12; accepted 2020 May 22; published 2020 June 17

Abstract

The magnetar Swift J1818.0–1607 was discovered in 2020 March when Swift detected a 9 ms hard X-ray burst and a long-lived outburst. Prompt X-ray observations revealed a spin period of 1.36 s, soon confirmed by the discovery of radio pulsations. We report here on the analysis of the Swift burst and follow-up X-ray and radio observations. The burst average luminosity was $L_{\rm burst} \sim 2 \times 10^{39}$ erg s^{-1} (at 4.8 kpc). Simultaneous observations with XMM-Newton and NuSTAR three days after the burst provided a source spectrum well fit by an absorbed blackbody ($N_{\rm H} = (1.13 \pm 0.03) \times 10^{23}$ cm^{-2} and $kT = 1.16 \pm 0.03$ keV) plus a power law ($\Gamma = 0.0 \pm 1.3$) in the 1–20 keV band, with a luminosity of $\sim 8 \times 10^{34}$ erg s^{-1}, dominated by the blackbody emission. From our timing analysis, we derive a dipolar magnetic field $B \sim 7 \times 10^{14}$ G, spin-down luminosity $\dot{E}_{\rm rot} \sim 1.4 \times 10^{36}$ erg s^{-1}, and characteristic age of 240 yr, the shortest currently known. Archival observations led to an upper limit on the quiescent luminosity $<5.5 \times 10^{33}$ erg s^{-1}, lower than the value expected from magnetar cooling models at the source characteristic age. A 1 hr radio observation with the Sardinia Radio Telescope taken about 1 week after the X-ray burst detected a number of strong and short radio pulses at 1.5 GHz, in addition to regular pulsed emission; they were emitted at an average rate 0.9 min^{-1} and accounted for ∼50% of the total pulsed radio fluence. We conclude that Swift J1818.0–1607 is a peculiar magnetar belonging to the small, diverse group of young neutron stars with properties straddling those of rotationally and magnetically powered pulsars. Future observations will make a better estimation of the age possible by measuring the spin-down rate in quiescence.

Unified Astronomy Thesaurus concepts: Magnetars (992); Neutron stars (1108); Transient sources (1851); X-ray bursts (1814); Radio pulsars (1353)

1. Introduction

The emission of magnetars is believed to be powered by the dissipation of their unstable strong magnetic fields ($B \sim 10^{14}$–10^{15} G; see Kaspi & Beloborodov 2017; Esposito et al. 2018 for recent reviews). At variance, in the vast majority of radio pulsars, rotational energy provides the energy budget for particle acceleration, ultimately leading to their radio to gamma-ray emission. However, a well-defined dichotomy between the two classes was shown to be inadequate. In particular, magnetar-like X-ray activity was found from pulsars with powerful rotational energy loss rate, such as PSR J1846−0258 (Gavriil et al. 2008) and PSR J1119−6127 (Archibald et al. 2016), whereas pulsed radio emission was detected from several magnetars in outburst. Moreover, enigmatic magnetars having dipolar magnetic fields as low as a few 10^{12} G (Rea et al. 2010, 2013) or spin periods of the order of a few hours (De Luca et al. 2006; Rea et al. 2016) were discovered. These findings hint at a complex, more compounded picture.

On 2020 March 12, the Burst Alert Telescope (BAT) on board the Neil Gehrels Swift Observatory (Gehrels et al. 2004) triggered on a burst, which was soon recognized to have characteristics typical of those of short bursts from magnetars (Evans et al. 2020). The Swift X-ray Telescope (XRT) started to observe the field about 64 s afterwards, and detected a new uncatalogued X-ray source, Swift J1818.0–1607 (henceforth dubbed Swift J1818). Follow-up observations with the Neutron star Interior Composition Explorer (NICER) detected a coherent periodic X-ray signal at 1.36 s (Enoto et al. 2020). Furthermore, radio observations from several antennas identified Swift J1818 as the fifth radio-loud magnetar (Karuppusamy et al. 2020) and provided a first measurement of the spin period derivative of 8.2×10^{-11} s s^{-1} (Champion et al. 2020), converting to a dipolar magnetic field of $B \sim 6.8 \times 10^{14}$ G and a very small characteristic age <300 yr.

This Letter reports on (i) the burst detected by Swift/BAT that led to the discovery of Swift J1818, (ii) prompt

Table 1
Observation Log

Instrument[a]	Obs.ID	Start	Stop	Exposure	Count Rate[b]
		YYYY-M-DD hh:mm:ss (TT)		(ks)	(counts s^{-1})
ROSAT/PSPC	50311	1993 Sep 12 20:55:04	1993 Sep 13 18:09:28	6.7	$<10^{-3}$
Chandra/ACIS-I (TE)	8160	2008 Feb 16 06:46:59	2008 Feb 16 07:51:04	2.7	$<2.5 \times 10^{-3}$
XMM/EPIC-pn (FF)	0152834501	2003 Mar 28 04:35:03	2003 Mar 28 07:26:37	8.4	<0.062
Swift/XRT (PC)	00032293013	2012 Mar 17 15:03:55	2012 Mar 17 15:25:56	1.3	<0.026
Swift/XRT (PC)	00044110002	2012 Oct 12 17:14:05	2012 Oct 12 17:16:55	0.2	<0.089
Swift/XRT (PC)	00044110003	2012 Oct 17 13:08:36	2012 Oct 17 13:11:55	0.2	<0.113
Swift/XRT (PC)	00044111003	2012 Oct 23 21:07:27	2012 Oct 23 21:12:56	0.3	<0.043
Swift/XRT (PC)	00087426001	2017 Jul 24 19:11:45	2017 Jul 24 21:00:52	2.2	$<8.1 \times 10^{-3}$
Swift/XRT (PC)	00087426002	2017 Jul 27 21:45:57	2017 Jul 27 23:37:52	2.7	$<4.9 \times 10^{-3}$
XMM/EPIC-pn (FF)	0800910101	2018 Apr 8 21:27:40	2018 Apr 9 14:24:19	60.4	$<8.3 \times 10^{-3}$
Swift/XRT (PC)	00960986000	2020 Mar 12 21:18:22	2020 Mar 12 21:36:48	1.1	0.15 ± 0.01
Swift/XRT (PC)	00960986001	2020 Mar 12 22:57:45	2020 Mar 13 05:13:02	4.9	0.14 ± 0.01
Swift/XRT (WT)	00960986002	2020 Mar 13 20:47:55	2020 Mar 13 21:21:15	2.0	0.16 ± 0.01
Swift/XRT (PC)	00960986003	2020 Mar 15 00:10:37	2020 Mar 15 03:36:52	1.5	0.14 ± 0.01
NuSTAR/FPMA	80402308002	2020 Mar 15 03:58:21	2020 Mar 15 15:58:03	22.2	0.443 ± 0.005
XMM/EPIC-pn (LW)	0823591801	2020 Mar 15 07:57:47	2020 Mar 15 14:41:12	22.1	1.45 ± 0.01
Swift/XRT (WT)	00960986004	2020 Mar 19 09:33:11	2020 Mar 19 11:16:56	1.7	0.19 ± 0.02
Swift/XRT (WT)	00960986005	2020 Mar 20 04:34:19	2020 Mar 20 04:49:56	1.8	0.20 ± 0.01
Swift/XRT (WT)	00960986006	2020 Mar 22 02:35:21	2020 Mar 22 03:01:56	1.6	0.16 ± 0.01
Swift/XRT (WT)	00960986007	2020 Mar 24 05:51:38	2020 Mar 24 09:02:56	1.2	0.13 ± 0.01
Swift/XRT (WT)	00960986008	2020 Mar 26 05:40:29	2020 Mar 26 23:20:56	1.1	0.19 ± 0.01
Swift/XRT (WT)	00960986009	2020 Mar 28 03:40:53	2020 Mar 28 18:07:56	1.2	0.18 ± 0.02
Swift/XRT (WT)	00960986010	2020 Mar 29 16:25:13	2020 Mar 30 21:03:56	1.3	0.16 ± 0.01
Swift/XRT (WT)	00960986011	2020 Apr 1 19:17:34	2020 Apr 1 19:25:56	0.5	0.17 ± 0.02

Notes.
[a] The instrumental setup is indicated in brackets: TE = timed exposure, FF = full frame, PC = photon counting, WT = windowed timing, and LW = large window.
[b] The count rate is in the 0.3–10 keV energy range, except for ROSAT (0.1–2.4 keV) and NuSTAR (3–20 keV); if the source was not detected, we give a 3σ upper limit.

simultaneous X-ray observations using XMM-Newton and NuSTAR, (iii) the Swift/XRT monitoring campaign over the first three weeks of the outburst, and (iv) radio observations with the Sardinia Radio Telescope (SRT) in the *P* (0.34 GHz) and *L* (1.5 GHz) bands, performed one week after the burst detection (Sections 2 and 3). Summary of the results and discussion follow (Section 4).

2. X-Ray Emission

2.1. Observations and Data Analysis

2.1.1. Swift

After the Swift/BAT detection of the burst and the prompt slew of the spacecraft (obs.ID 00960986000), several Swift/XRT observations of Swift J1818 were carried out, in both photon counting (PC; charge-coupled device (CCD) readout time of 2.5 s) and windowed timing (WT; readout time of 1.8 ms) modes (see Table 1). The data were processed and analyzed using standard procedures and software packages (HEASOFT v. 6.25, CALDB 2020 January 9). The source photons were selected within a 20 pixel radius (1 pixel $=2\farcs36$). Swift/BAT mask-tagged light curves, images and spectra were created only for the burst event.

2.1.2. XMM-Newton

Swift J1818 was observed with the European Photon Imaging Camera (EPIC) on board the XMM-Newton satellite on 2020 March 15 for an on-source exposure time of 22.1 ks (Table 1). The EPIC-pn (Strüder et al. 2001) was set in large window mode (LW; timing resolution of 47.7 ms), while both MOS detectors (Turner et al. 2001) were operating in small window (SW; timing resolution of 0.3 s) mode. In this Letter, we use only the data acquired with the EPIC-pn camera, owing to its higher time resolution and better capability to model diffuse emission around the source (Section 2.2.2) compared to the central CCD of the MOS operated in SW. The raw data were analyzed with the SAS v. 18.0.0 software package. We cleaned the observations from periods of high background activity; in the EPIC-pn, this resulted in a net exposure of 14 ks.

We detected diffuse emission around the source (Figure 1). To quantify its spatial extension, we extracted the radial profile of the observed surface brightness up to a radial distance of $300''$ from the source. We then modeled it using a King function reproducing the EPIC-pn point-spread function (PSF; Ghizzardi 2002) plus a constant term accounting for the background level. A photon excess associated with the diffuse emission is present at radial distances within the $\approx 50''$–$110''$ range (Figure 1). We selected the source photon counts from a circle of $40''$ radius, and those of the diffuse emission from an annulus with radii of $50''$ and $110''$. The background level was estimated using a $100''$ circle far from the source, on the same CCD. The average background-subtracted surface brightness of the diffuse emission was (0.086 ± 0.002) counts arcsec^{-2} (0.3–10 keV).

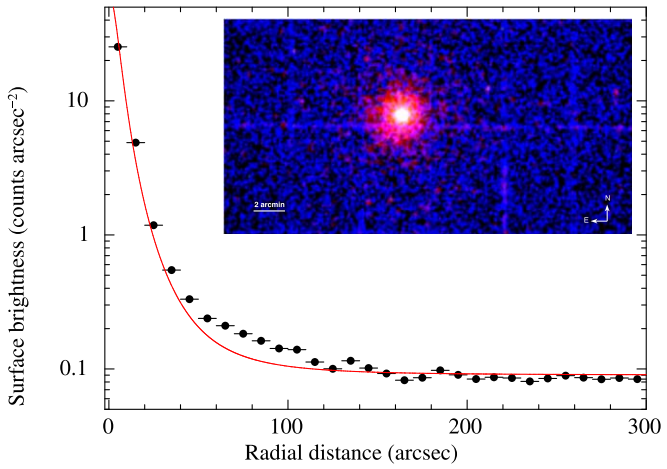

Figure 1. Observed X-ray surface brightness up to a radial distance of 300″ from the source in the 0.3–10 keV energy range (note that the error bars are smaller than the symbols). The red curve represents the PSF model. The inset shows a false-color X-ray image from the EPIC-pn observation. Red, green, and blue colors correspond to the 2–4, 4–7.5, and 8.5–12 keV energy bands, respectively.

2.1.3. NuSTAR

NuSTAR (Harrison et al. 2013) observed Swift J1818 on 2020 March 15 for an on-source exposure time of 22.2 ks (Table 1). We reprocessed the event lists and filtered out passages of the satellite through the South Atlantic Anomaly using the NUPIPELINE script in the NUSTARDAS 1.9.3 package with the latest calibration files (v. 20200429). Stray-light contamination from a source outside the field of view is evident for both modules, but particularly strong in the FPMB data. Swift J1818 was detected up to ∼20 keV and ∼15 keV in the FPMA and FPMB, respectively. A circle with a radius of 100″ was used to collect source photons (∼90% enclosed energy fraction; Madsen et al. 2015), while background counts were extracted from a 100″ circle located on the same chip as the target. To study the source emission up to the highest energies we used only the data from the FPMA. We extracted light curves and spectra and generated instrumental response files using NUPRODUCTS.

2.2. Results of the X-Ray Analysis

2.2.1. Burst Properties

The burst had a T90 duration (the time interval containing 90% of the counts) of 8 ± 2 ms and a total duration of ∼9 ms. These values were computed by the Bayesian blocks algorithm BATTBLOCKS on mask-weighted light curves binned at 1 ms in the 15–150 keV range (the light curve of the event is shown in Figure 2), where essentially all the emission is contained.

We tested a blackbody, a power law, and an optically thin thermal bremsstrahlung to the time-averaged spectrum. All models provided good fits, with reduced χ^2, $\chi^2_\nu = 0.62$ for 56 degrees of freedom (dof) in the case of a blackbody (temperature of $kT = 6.4 \pm 0.7$ keV), $\chi^2_\nu = 0.70/56$ dof for the power law (photon index $\Gamma = 3.1^{+0.3}_{-0.2}$), and $\chi^2_\nu = 0.65/56$ dof for the bremsstrahlung ($kT = 21^{+5}_{-4}$ keV). From the blackbody fit we found an average flux $(6.2 \pm 0.9) \times 10^{-7}$ erg cm^{-2} s^{-1} in the 15–150 keV range, corresponding to an isotropic luminosity of $(1.7 \pm 0.3) \times 10^{39} d^2_{4.8}$ erg s^{-1}, where $d_{4.8}$ is the source distance in units of 4.8 kpc (Karuppusamy et al. 2020).

2.2.2. Persistent Emission

The XMM-Newton/EPIC-pn and NuSTAR/FPMA background-subtracted spectra were grouped so as to have at least 100 and 50 counts per bin, respectively. The spectral analysis was performed with XSPEC. Absorption by the interstellar medium was modeled using the TBABS model with the abundances from Wilms et al. (2000). We extracted the spectra in the 0.3–10 keV range but, after inspecting the data, we limited the analysis to the 1–10 keV energy range, because of the very low signal-to-noise ratio (S/N) of Swift J1818 below 1 keV.

First, we fit the EPIC-pn spectrum of the diffuse emission with an absorbed blackbody model, deriving a temperature $kT_{\rm diff} = (0.88 \pm 0.02)$ keV. We then modeled the Swift J1818 EPIC-pn spectrum with two absorbed blackbody components, by fixing the first temperature to $kT_{\rm diff}$ and leaving all normalizations free to vary. We derived a column density of $N_{\rm H} = (1.12 \pm 0.03) \times 10^{23}$ cm^{-2}, a source temperature of $kT_{\rm BB} = (1.17 \pm 0.03)$ keV and an emitting radius of $R_{\rm BB} = (0.57 \pm 0.02)$ km (at 4.8 kpc). The observed fluxes of the source and diffuse blackbody components in the 1–10 keV range were $F_{\rm BB} \sim 1.4 \times 10^{-11}$ erg cm^{-2} s^{-1}, and $F_{\rm diff} \sim 4 \times 10^{-13}$ erg cm^{-2} s^{-1}, respectively. At a distance of 4.8 kpc this corresponds to a source luminosity of $\sim 7 \times 10^{34} d^2_{4.8}$ erg s^{-1}.

We then performed a joint fit of the EPIC-pn and FPMA spectra using the above-mentioned model plus a power-law component to model the source high-energy emission. We removed the FPMA data below 8 keV to minimize contamination from diffuse emission at lower energies. All parameters were tied between the two spectra. The best-fitting values resulted: $N_{\rm H} = (1.13 \pm 0.03) \times 10^{23}$ cm^{-2}, $kT = (1.16 \pm 0.03)$ keV, $R_{\rm BB} = (0.58 \pm 0.03)$ km (at 4.8 kpc) and photon index $\Gamma = 0.0 \pm 1.3$ ($\chi^2_\nu = 1.1$ for 109 dof; see Figure 2). The total observed flux after subtracting the contribution from the diffuse emission was $\sim 1.5 \times 10^{-11}$ erg cm^{-2} s^{-1} (1–20 keV), giving a luminosity of $\sim 8 \times 10^{34} d^2_{4.8}$ erg s^{-1} (1–20 keV). The observed flux of the blackbody component was $\sim 1.3 \times 10^{-11}$ erg cm^{-2} s^{-1} (1–20 keV), accounting for most of the observed X-ray emission, and corresponding to a luminosity of $\sim 6.8 \times 10^{34} d^2_{4.8}$ erg s^{-1} (1–20 keV).

Given the short exposure, poor statistics and S/N of the Swift/XRT observations, their analysis was mainly aimed at sampling the long-term flux evolution of Swift J1818, and supplementing the XMM-Newton and NuSTAR timing analysis. For this reason, we fit simultaneously all the Swift spectra with an absorbed blackbody model ($N_{\rm H}$ was kept frozen at the above-mentioned value). Figure 2 shows the long-term light curve of Swift J1818. From the XMM-Newton spectral analysis, we estimate that the systematic uncertainty of fluxes and luminosities resulting from contamination by the diffuse emission is $\lesssim$15% (if steady in time).

The field of Swift J1818 was observed several times with sensitive imaging instruments before 2020 March (Table 1; Mereghetti et al. 2012). The source was not detected in any observation (see Table 1 for the 3 σ upper limits on the count rate). The Chandra and the 2018 XMM-Newton observations provided the deepest limits. Using the WEBPIMMS tool[16] and assuming an absorbed blackbody with $kT = 0.3$ keV and $N_{\rm H} = 1.\ 2 \times 10^{23}$ cm^{-2}, both their limits translate into a

[16] See https://heasarc.gsfc.nasa.gov/cgi-bin/Tools/w3pimms/w3pimms.pl.

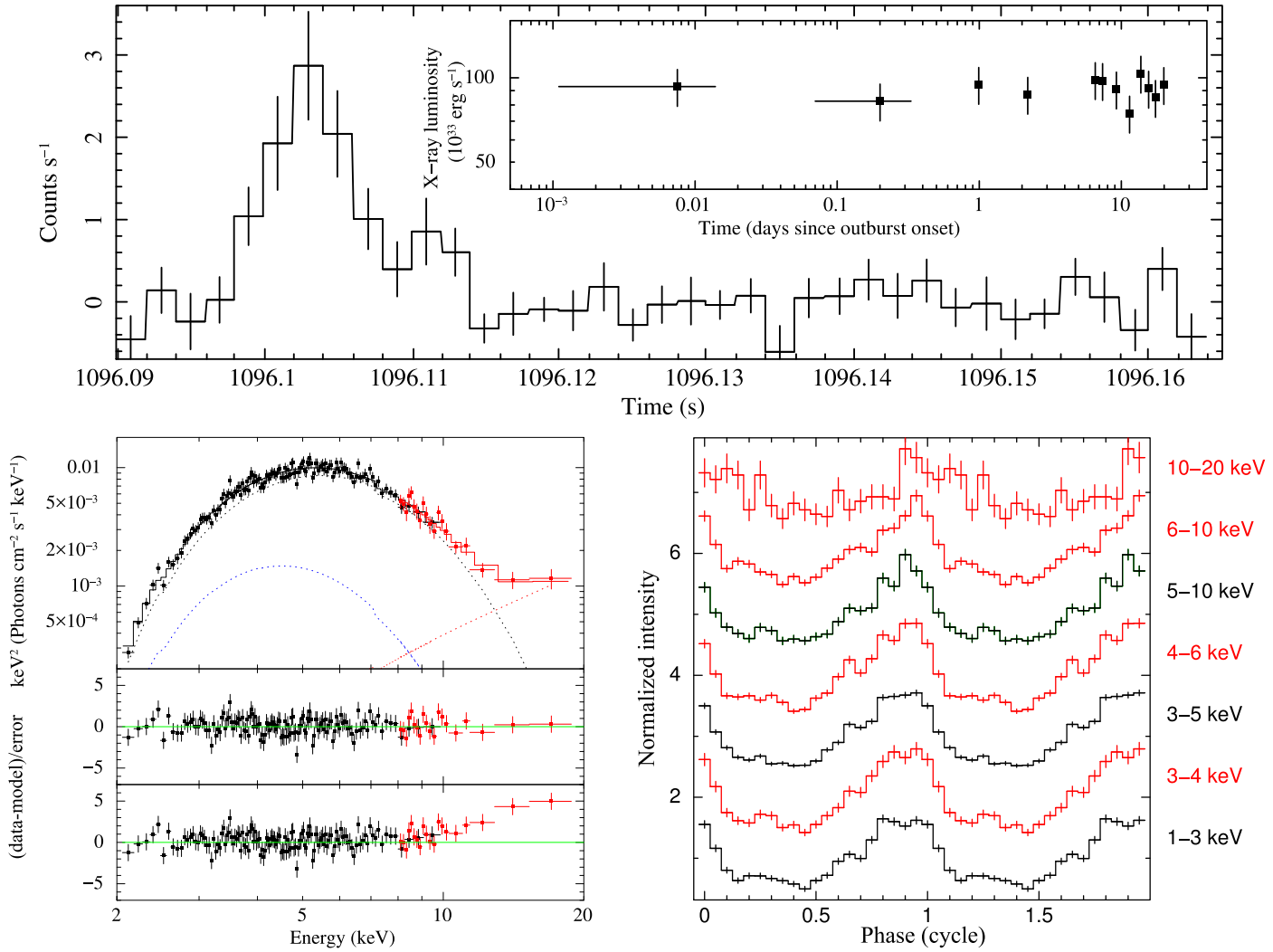

Figure 2. Top panel: BAT light curve (15–150 keV, bin time: 2 ms; the start time is arbitrary). The inset shows the evolution of the 0.3–10 keV luminosity of Swift J1818 measured with Swift/XRT since the burst trigger (MJD 58,920.8867). Bottom-left panel, top: broadband unfolded spectrum extracted from the simultaneous XMM-Newton/EPIC-pn (in black) and NuSTAR/FPMA (red) data. The solid line shows the best-fitting model. The blue, black, and red dotted lines indicate the diffuse emission component, the source blackbody and power-law components, respectively. Bottom-left panel, middle: post-fit residuals. Bottom-left panel, bottom: residuals after removing the power-law component from the model. Bottom-right panel: energy-resolved pulse profiles of Swift J1818 extracted from the EPIC-pn (in black) and NuSTAR/FPMA (red) data.

0.3–10 keV flux of $<3.4 \times 10^{-14}$ erg cm^{-2} s^{-1}, corresponding to a luminosity of $<5.5 \times 10^{33} d_{4.8}^2$ erg s^{-1}. We also note that in the 2018 XMM-Newton observation, the diffuse emission was not detectable, with an upper limit implying an emission at least ∼10 times fainter (A. Tiengo et al. 2020, in preparation).

2.2.3. Timing Analysis

For the timing analysis, we referred the photon arrival times to the solar system barycenter using our best Swift position (R.A.=$18^h18^m00^s.16$, decl.=$-16°07'53''.2$, J2000.0; uncertainty of $2''$ at 90% c.l.). By a phase-fitting analysis of the X-ray data, we measured a period $P = 1.363489(3)$ s and a period derivative $\dot{P} = 9(1) \times 10^{-11}$ s s^{-1} (with epoch MJD 58,922.31 and valid over the MJD range 58,923.5–58,928.5), compatible with previous radio timing measurements reported by Champion et al. (2020). The energy-resolved pulse profiles extracted from EPIC-pn and NuSTAR data are shown in Figure 2. The background-subtracted peak-to-peak semi-amplitude increases with energy from (52 ± 2)% to (66 ± 2)% over the 1–10 keV band (as measured with the EPIC-pn), and is equal to (58 ± 13)% in the 10–20 keV range. The latter values are not corrected for the underlying diffuse emission component, which should affect the pulsed fraction values by a few percents.

3. Radio Emission

We observed Swift J1818 with the SRT on 2020 March 19 at 05:05 UTC for 1 hr, using the coaxial L/P band receiver to observe simultaneously in two frequency bands, centered at 1548 MHz and 336 MHz, respectively. In the L band, we recorded the total intensity signal in incoherent search mode over a usable bandwidth of ∼390 MHz with frequency resolution of 1 MHz and time resolution of 100 μs. We de-dispersed and folded the data using our position of the source and the spin parameters and dispersion measure (DM) by Champion et al. (2020). We extracted topocentric times-of-arrival and used them to determine the DM = 700.8(6) pc cm^{-3}, the spin frequency $\nu = 0.7333920(2)$ Hz ($P = 1.3635273(4)$ s, compatible within 1σ uncertainty with the measurement of Champion et al. (2020) and the pulse

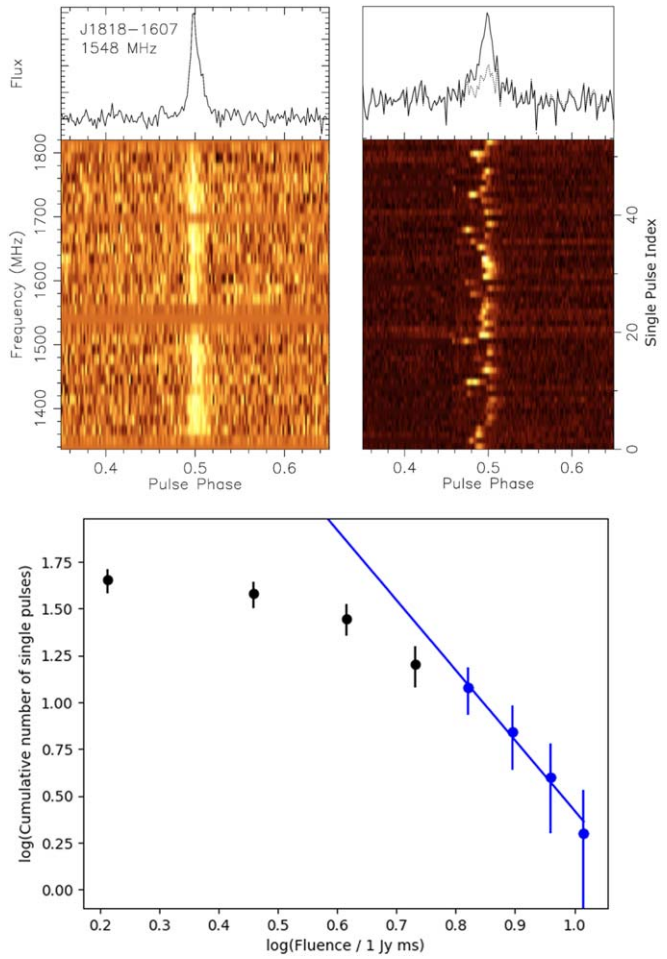

Figure 3. Top-left panel: profile of the strongest single pulse detected with the SRT (the flux is in arbitrary units) de-dispersed at a DM = 700.8 pc cm^{-3} (top) and waterfall plot (below) displaying the observing frequency (in 30 × 16 MHz wide sub-bands) vs. the pulse phase (which is arbitrary with respect to the X-ray pulse phase of Figure 2) for the same single pulse as the panel above. Top-right panel: the integrated pulse profile over the entire observation, lasting about 1 hr (solid line), as well as the integrated profile after removing from the profile above the 53 strong single pulses mentioned in the text (dotted line). The two profiles of the top row are reported with the same phase reference (also identical to that of the left panel) of the detected series of the 53 single pulses, which are plotted below, on a color scale, on top of each other. Although not arriving at a constant rotational phase, the latter are basically confined within the phase range of the total integrated pulse profile. Bottom panel: cumulative number of single pulses exceeding a given fluence. The uncertainties are considered to be those of a Poisson process. The line shows the power-law fit to the blue points.

profile width (at 50% of the peak) $W50 \sim 40$ ms at epoch MJD 58,927.23. The optimized S/N ∼ 22 of the SRT observation implies an average flux density $S_{\rm ave} \sim 0.2$ mJy, assuming an antenna gain 0.55 K Jy^{-1} and system temperature ∼30 K during the observation ($S_{\rm ave}$ and all the energetic/fluence calculation below must be considered as a lower limit as the residual in-band RFI can have a significant impact on the value of the rms noise).

A search for single pulses was carried out with PRESTO[17] (Ransom 2001). The data were down-sampled by a factor of four and de-dispersed at the above DM. The script SINGLE_PULSE_SEARCH.PY was run with S/N threshold of 8 and maximum width of 0.1 s, unveiling 53 pulses (Figure 3). Their widths ($W50_{\rm SP}$) range from ∼7 to ∼22 ms (significantly smaller than the width of the integrated profile) and their PDMP[18] S/N's range from 7 to 37. The energetic per rotation $E_{\rm SP}$ (the pulse-integrated flux density using a pulse width at 50% of the peak and averaged over a spin period) of each single pulse was determined from the values above and compared with the average energetic per rotation of the radio emission $E_{\rm no\text{-}SP}$, after removing the rotations containing the aforementioned single pulses. We found a ratio $R_{\rm E} = E_{\rm SP}/E_{\rm no\text{-}SP}$ ranging from 16 to 126.

In the *P* band, we collected baseband data over a bandwidth of 64 MHz. After coherently de-dispersing and folding, we could not detect any pulsations from Swift J1818. This can be ascribed to scattering of the radio signal by the interstellar medium. Indeed, evidence of scattering was seen in the lower part of the *L* band by other telescopes (Joshi & Bagchi 2020; Lower et al. 2020), which report scattering timescales of $\tau_s \sim 44$ ms at 1 GHz and ∼500 ms at 600 MHz. These imply $\tau_s \sim 3.5$ s at 336 MHz, hence pulsations in the *P* band are likely completely smeared out.

Finally, we searched for Swift J1818 in archival Parkes data. We found one observation at offset of 2.′9 taken on 1998 August 1 at 1374 MHz. No pulsations down to a S/N = 7 were detected, implying an upper limit to the flux density of 0.12 mJy.

4. Discussion

With a spin period of 1.36 s, Swift J1818 is among the fastest magnetars, in between the very active magnetar 1E 1547.0–5408 (2.1 s, also a radio emitting one; Camilo et al. 2007) and the allegedly rotation-powered pulsars PSR J1846–0258 (0.33 s) and PSR J1119–6127 (0.41 s), which underwent magnetar-like outbursts (Gavriil et al. 2008; Archibald et al. 2016).

Our X-ray timing measurements of Swift J1818 can be used to infer (i) the characteristic age $\tau_c = P/(2\dot{P}) \simeq 240$ yr, (ii) the spin-down luminosity $\dot{E}_{\rm rot} = 4\pi^2 I \dot{P} P^{-3} \simeq 1.4 \times 10^{36}$ erg s^{-1}, assuming a moment of inertia $I \approx 10^{45}$ g cm^2, and (iii) the intensity of the dipolar component of the magnetic field at the pole, $B \approx 6.4 \times 10^{19} (P\dot{P})^{1/2} \simeq 7 \times 10^{14}$ G using the classical formula for an orthogonal rotator in vacuum. These values are compatible with the results from radio timing (Champion et al. 2020). With $\tau_{\rm c} = 240$ yr, Swift J1818 possibly represents the youngest pulsar discovered to date in the Galaxy, seconded by PSR J1846–0258. However, we caution that the age of Swift J1818, apart from the uncertainties connected to similar estimates, needs confirmation by a $\dot{P}$ measurement during quiescence and by the detection of its supernova remnant.

The observed 9 ms burst with average luminosity $L_{\rm burst} \sim 2 \times 10^{39} d_{4.8}^2$ erg s^{-1} (Section 2.2), and a persistent X-ray spectrum at the outburst peak modeled by a blackbody of ∼1 keV and a dim nonthermal component, are commonly seen during magnetar outbursts (e.g., Coti Zelati et al. 2018). The radio emission of Swift J1818 is not dissimilar to what observed in other radio magnetars. The period measured with SRT in radio is compatible within 3σ with our X-ray timing parameters (Section 2.2.3). The fluence distribution of the strongest single pulses can also be fit with a power law having index -3.7 ± 0.3 (1σ uncertainty, Figure 3). This, together with the fact that $W50_{\rm SP} \ll W50$, and with the high values of

[17] http://www.cv.nrao.edu/~sransom/presto/

[18] http://psrchive.sourceforge.net

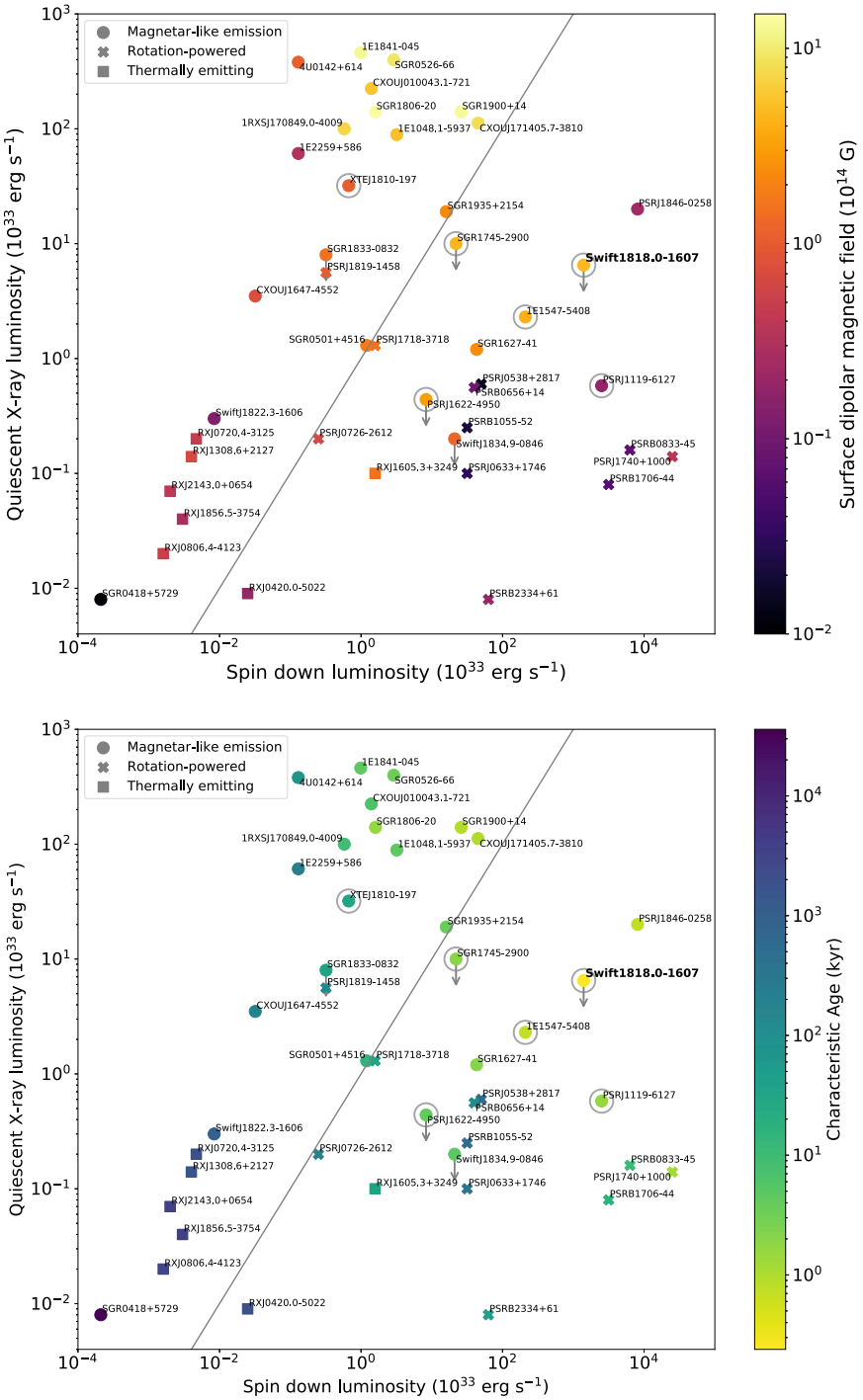

Figure 4. Quiescent X-ray luminosity as a function of the spin-down power for different classes of isolated X-ray pulsars, including Swift J1818 (in bold). Circles denote radio-loud magnetars. The gray line indicates the equality line for the two parameters. Markers are color-coded according to the strength of the dipolar magnetic field at the pole (top) and the characteristic age (bottom). Values are from the Magnetar Outburst Online Catalogue (http://magnetars.ice.csic.es/; Coti Zelati et al. 2018), with updates for PSR 1622−4950 and SGR 1806−20 (Younes et al. 2017; Camilo et al. 2018).

R_E, are all reminiscent of the giant pulses observed in dozens of radio pulsars (e.g., Oronsaye et al. 2015).

The ratio $S_{SP}/S_{ave} \sim 0.50$, where S_{SP} is the average flux density associated to the sum of the 53 single pulses, is independent of the uncertain flux calibration (Section 3), and implies that at least 50% of the total energy of the radio emission from Swift J1818 is released in a form which resembles that of giant pulses. They have an average cadence of ∼0.9 minute^{-1} (one burst every ∼50 rotations) and fluence larger than 1.3 Jy ms. This means that, at the time of the SRT observation, the underlying radio emission mechanisms of Swift J1818 were dominated by the sporadic emission of a succession of strong single radio bursts (with a flux density 1–2 orders of magnitude larger than the average flux density of the remaining pulsed emission), in contrast to what is typically seen in ordinary radio pulsars. Interestingly, if the source had been located 2–3 times farther, the regular pulsed emission could have been completely undetectable and the sporadic

strong pulses interpreted as emitted by a rotating radio transient (RRAT; McLaughlin et al. 2006), for some of which a link with the magnetar population has been proposed (Lyne et al. 2009; Rea et al. 2009). According to observations taken 12 days later at Parkes (Lower et al. 2020), the SRT pointing could have captured a transient behavior of Swift J1818, in agreement with the highly variable phenomenology shown also by other radio magnetars.

Figure 4 shows the quiescent X-ray luminosity (estimated as explained by Coti Zelati et al. 2018), as a function of the spin-down luminosity for all neutron stars (NSs) that showed magnetar-like emission, some high-B radio pulsars with detected X-ray emission, and the isolated thermally emitting NSs (Turolla 2009). This figure shows that the balance between magnetic energy (related to the quiescent luminosity) and rotational power might differ considerably between different sources of the same class. Most of the radio magnetars can count on large rotational energy (Rea et al. 2012), and this is also the case for Swift J1818. The X-ray nonthermal luminosity in quiescence expected from the empirical $L_{\rm X}$–$\dot{E}_{\rm rot}$ relation for rotation-powered X-ray pulsars by Shibata et al. (2016) is $L_{\rm X} = 3^{+2}_{-1} \times 10^{32}$ erg s^{-1} (0.5–10 keV). This value is consistent with the non-detection in the archival data (Table 1), but much smaller than the outburst value, $8 \times 10^{34} d^2_{4.8}$ erg s^{-1} (Section 2.2.2). The X-ray conversion factor is $L_{\rm X}/\dot{E}_{\rm rot} < 1$ in quiescence, and even at the outburst peak.

NSs with true age of a few centuries are expected to be still hot, with thermal luminosity normally exceeding 10^{34} erg s^{-1} (Pons et al. 2009; Viganò et al. 2013). Moreover, when high magnetic fields are taken into account, the Joule dissipation of the currents in the crust keeps the surface even hotter. According to crustal-confined magnetic field evolutionary models (Viganò et al. 2013), we should expect a minimum quiescent thermal luminosity of at least $L_{\rm qui} = (5–7) \times 10^{34}$ erg s^{-1}, or even higher if the NS has an envelope of light-elements, or the magnetic field has additional small scales components and/or a toroidal component.

The value that we derive for the quiescent luminosity of Swift J1818 is $<10^{34} d^2_{4.8}$ erg s^{-1} (see Figure 4), rather low given the magnetic field ($B \lesssim 10^{14}$ G) of this young magnetar. This can be explained if (a) the current $\dot{P}$ value is higher than in quiescence due to the extra-torque that might act during the outburst, as observed in other magnetars (e.g., Livingstone et al. 2011), thus implying that the real age is actually larger than 240 yr; (b) currents are living only in the core, there are no toroidal components, and the NS underwent a fast cooling phase (meaning direct URCA processes and/or early superfluid transition; e.g., Page et al. 2011); or (c) the source is farther than estimated from the DM. In this respect, we note that distances inferred from the DM have large uncertainties for individual objects, and in the case of Swift J1818, the value also strongly depends on the model for the Galactic electron density, 4.8 kpc using the YMW16 model (Yao et al. 2017) and 8.1 kpc with the NE2001 (Cordes & Lazio 2002).

Our future observations of the evolution of the source toward quiescence will help to address whether the diffuse emission surrounding the source is a dust scattering halo due to the bursting activity or the brightening of Swift J1818 (see Tiengo et al. 2010), as well as to constrain the quiescent spin-down rate.

Overall, we see the emission observed from Swift J1818 as another example of the possible ubiquitous presence of magnetar-like activity in pulsars of any class.

This research is based on observations with XMM-Newton (ESA/NASA), NuSTAR (CaltTech/NASA/JPL), Swift (NASA/ASI/UKSA), and on data retrieved through the CXC and the NASA/GSFCs HEASARC archives. We acknowledge the support of the PHAROS COST Action (CA16214). N.R., A.B., D.V., C.D., M.R., A.G.G., and V.G. are supported by the ERC Consolidator grant "MAGNESIA" (No. 817661) and acknowledge funding from grants SGR2017-1383 and PGC2018-095512-BI00. A.B. and F.C.Z. are also supported by a Juan de la Cierva fellowship. G.L.I., S.M., A.T., and R.T. acknowledge financial support from the Italian MIUR through PRIN grant 2017LJ39LM. A.P., A.R., M.B., and L.S. acknowledge funding from the grant "iPeska" (INAF PRIN-SKA/CTA; PI Possenti). L.S. acknowledges funding from ASI-INAF agreements 2017-14-H.O and I/037/12/0.

Facilities: XMM-Newton (EPIC), Swift (BAT, XRT), NuSTAR, SRT.

Software: SAS (Gabriel et al. 2004), FTOOLS (Blackburn 1995), XSPEC (Arnaud 1996), NuSTARDAS, PRESTO.

ORCID iDs

P. Esposito https://orcid.org/0000-0003-4849-5092
N. Rea https://orcid.org/0000-0003-2177-6388
A. Borghese https://orcid.org/0000-0001-8785-5922
F. Coti Zelati https://orcid.org/0000-0001-7611-1581
D. Viganò https://orcid.org/0000-0001-7795-6850
G. L. Israel https://orcid.org/0000-0001-5480-6438
A. Tiengo https://orcid.org/0000-0002-6038-1090
A. Ridolfi https://orcid.org/0000-0001-6762-2638
A. Possenti https://orcid.org/0000-0001-5902-3731
M. Burgay https://orcid.org/0000-0002-8265-4344
F. Pintore https://orcid.org/0000-0002-3869-2925
L. Stella https://orcid.org/0000-0002-0018-1687
C. Dehman https://orcid.org/0000-0003-0554-7286
S. Campana https://orcid.org/0000-0001-6278-1576
A. Garcia-Garcia https://orcid.org/0000-0002-9575-6403
V. Graber https://orcid.org/0000-0002-6558-1681
S. Mereghetti https://orcid.org/0000-0003-3259-7801
R. Perna https://orcid.org/0000-0002-3635-5677
G. A. Rodríguez Castillo https://orcid.org/0000-0003-3952-7291
R. Turolla https://orcid.org/0000-0003-3977-8760
S. Zane https://orcid.org/0000-0001-5326-880X

References

Archibald, R. F., Kaspi, V. M., Tendulkar, S. P., & Scholz, P. 2016, ApJL, 829, L21
Arnaud, K. A. 1996, in ASP Conf Ser. 101, Astronomical Data Analysis Software and Systems V, XSPEC: The First Ten Years, ed. G. H. Jacoby & J. Barnes (San Francisco, CA: ASP), 17
Blackburn, J. K. 1995, in ASP Conf. Ser. 77, Astronomical Data Analysis Software and Systems IV., FTOOLS: A FITS Data Processing and Analysis Software Package, ed. R. A. Shaw, H. E. Payne, & J. J. E. Hayes (San Francisco, CA: ASP), 367
Camilo, F., Ransom, S. M., Halpern, J. P., & Reynolds, J. 2007, ApJL, 666, L93
Camilo, F., Scholz, P., Serylak, M., et al. 2018, ApJ, 856, 180
Champion, D., Desvignes, G., Jankowski, F., et al. 2020, ATel, 13559, 1
Cordes, J. M., & Lazio, T. J. W. 2002, arXiv:astro-ph/0207156

Coti Zelati, F., Rea, N., Pons, J. A., Campana, S., & Esposito, P. 2018, MNRAS, 474, 961
De Luca, A., Caraveo, P. A., Mereghetti, S., Tiengo, A., & Bignami, G. F. 2006, Sci, 313, 814
Enoto, T., Sakamoto, T., Younes, G., et al. 2020, ATel, 13551, 1
Esposito, P., Rea, N., & Israel, G. L. 2018, in Timing Neutron Stars: Pulsations, Oscillations and Explosions, ed. T. Belloni, M. Mendez, & C. Zhang (Berlin: Springer) in press (arXiv:1803.05716)
Evans, P. A., Gropp, J. D., Kennea, J. A., et al. 2020, GCN, 27373, 1
Gabriel, C., Denby, M., Fyfe, D. J., et al. 2004, in ASP Conf. Ser. 314, Astronomical Data Analysis Software and Systems (ADASS) XIII, The XMM-Newton SAS—Distributed Development and Maintenance of a Large Science Analysis System: A Critical Analysis, ed. F. Ochsenbein, M. G. Allen, & D. Egret (San Francisco, CA: ASP), 759
Gavriil, F. P., Gonzalez, M. E., Gotthelf, E. V., et al. 2008, Sci, 319, 1802
Gehrels, N., Chincarini, G., Giommi, P., et al. 2004, ApJ, 611, 1005
Ghizzardi, S. 2002, XMM-Newton Calibration Rep. EPIC-MCT-TN-012
Harrison, F. A., Craig, W. W., Christensen, F. E., et al. 2013, ApJ, 770, 103
Joshi, B. C., & Bagchi, M. 2020, ATel, 13580, 1
Karuppusamy, R., Desvignes, G., Kramer, M., et al. 2020, ATel, 13553, 1
Kaspi, V. M., & Beloborodov, A. M. 2017, ARA&A, 55, 261
Livingstone, M. A., Scholz, P., Kaspi, V. M., Ng, C.-Y., & Gavriil, F. P. 2011, ApJL, 743, L38
Lower, M. E., Shannon, R. M., Johnston, S., & Bailes, M. 2020, ApJL, in press (arXiv:2004.11522)
Lyne, A. G., McLaughlin, M. A., Keane, E. F., et al. 2009, MNRAS, 400, 1439
Madsen, K. K., Harrison, F. A., Markwardt, C. B., et al. 2015, ApJS, 220, 8
McLaughlin, M. A., Lyne, A. G., Lorimer, D. R., et al. 2006, Natur, 439, 817
Mereghetti, S., Esposito, P., Tiengo, A., et al. 2012, A&A, 546, A30
Oronsaye, S. I., Ord, S. M., Bhat, N. D. R., et al. 2015, ApJ, 809, 51
Page, D., Prakash, M., Lattimer, J. M., & Steiner, A. W. 2011, PhRvL, 106, 081101
Pons, J. A., Miralles, J. A., & Geppert, U. 2009, A&A, 496, 207
Ransom, S. M. 2001, PhD thesis, Harvard Univ.
Rea, N., Borghese, A., Esposito, P., et al. 2016, ApJL, 828, L13
Rea, N., Esposito, P., Turolla, R., et al. 2010, Sci, 330, 944
Rea, N., Israel, G. L., Pons, J. A., et al. 2013, ApJ, 770, 65
Rea, N., Israel, G. L., Turolla, R., et al. 2009, MNRAS, 396, 2419
Rea, N., Pons, J. A., Torres, D. F., & Turolla, R. 2012, ApJL, 748, L12
Shibata, S., Watanabe, E., Yatsu, Y., Enoto, T., & Bamba, A. 2016, ApJ, 833, 59
Strüder, L., Briel, U., Dennerl, K., et al. 2001, A&A, 365, L18
Tiengo, A., Vianello, G., Esposito, P., et al. 2010, ApJ, 710, 227
Turner, M. J. L., Abbey, A., Arnaud, M., et al. 2001, A&A, 365, L27
Turolla, R. 2009, in Neutron Stars and Pulsars, ed. W. Becker (Heidelberg: Springer), 141
Viganò, D., Rea, N., Pons, J. A., et al. 2013, MNRAS, 434, 123
Wilms, J., Allen, A., & McCray, R. 2000, ApJ, 542, 914
Yao, J. M., Manchester, R. N., & Wang, N. 2017, ApJ, 835, 29
Younes, G., Baring, M. G., Kouveliotou, C., et al. 2017, ApJ, 851, 17